Mathematical and Computational Applications

Article

Finite Element Analysis of Hierarchical Metamaterial-Based Patterns for Generating High Expansion in Skin Grafting

Vivek Gupta [1] and Arnab Chanda [1,2,*]

[1] Centre for Biomedical Engineering, Indian Institute of Technology (IIT), Delhi 110016, India; bmz198618@iitd.ac.in
[2] Department of Biomedical Engineering, All India Institute of Medical Sciences (AIIMS), Delhi 110029, India
* Correspondence: arnab.chanda@cbme.iitd.ac.in; Tel.: +91-11-2659-1086(O)

Abstract: Burn injuries are very common due to heat, accidents, and fire. Split-thickness skin grafting technique is majorly used to recover the burn sites. In this technique, the complete epidermis and partial dermis layer of the skin are used to make grafts. A small amount of skin is passed into the mesher to create an incision pattern for higher expansion. These grafts are transplanted into the burn sites with the help of sutures for recovering large burn areas. Presently, the maximum expansion possible with skin grafting is very less (<3), which is insufficient for covering larger burn area with a small amount of healthy skin. This study aimed to determine the possibility of employing innovative auxetic skin graft patterns and traditional skin graft patterns with three levels of hierarchy. Six different hierarchical skin graft designs were tested to describe the biomechanical properties. The meshing ratio, Poisson's ratio, expansion, and induced stresses were quantified for each graft model. The computational results indicated that the expansion potential of the 3rd order auxetic skin graft was highest across all the models. These results are expected to improve burn surgeries and promote skin transplantation research.

Keywords: burn; skin; graft; hierarchical structures; metamaterials; expansion

Citation: Gupta, V.; Chanda, A. Finite Element Analysis of Hierarchical Metamaterial-Based Patterns for Generating High Expansion in Skin Grafting. *Math. Comput. Appl.* **2023**, *28*, 89. https://doi.org/10.3390/mca28040089

Academic Editor: Fábio Fernandes

Received: 5 June 2023
Revised: 13 July 2023
Accepted: 17 July 2023
Published: 1 August 2023

1. Introduction

Skin is wide spared, regulates temperature, defends against trauma, and preserves the internal organs from the outer environment. [1,2]. There are three layers of skin arranged as follows: the topmost layer is the epidermis, followed by the dermis in the middle, and finally, the hypo-dermis at the bottom [1,3–5]. Every year, millions of people suffer from severe and mild burns [6]. Burn injuries are a common occurrence and can result from various causes, such as fires, electric shock, hot liquids, and chemicals. These burns can cause damage to the skin and underlying tissues, leading to pain, inflammation, and impaired healing. One of the treatment options for managing burn injuries is grafting [7,8]. Meek skin grafting and traditional skin grafting techniques are two methods used in the field of plastic surgery to repair or reconstruct skin defects caused by burns, injuries, or diseases [9,10]. The Meek technique is an invasive procedure used to treat burn wounds that involve a large surface area of the body. It involves taking an ultra-thin layer of the skin, called a micrograft, from a donor site and expanding it in vitro by placing it in a special tissue culture solution [9,11]. The micrografts multiply and grow into a large sheet of skin called a Meek sheet. The Meek sheet is then placed on the wound site, where it integrates and grows into the surrounding tissue. In the traditional skin grafting method, a healthy portion of the skin is extracted, and several parallel incisions are developed using a meshing device and replaced with burn sites. Mostly, skin grafting in split-thickness mode involves creating parallel incisions on collected healthy skin to create a mesh-like pattern with small openings, which can then be used to cover a larger area of damaged skin [12]. There are several advantages and disadvantages of the Meek technique over traditional skin grafting. Meek skin grafting uses ultra-thin micrografts that require a smaller donor site, which can be advantageous in patients with limited donor sites. Meek skin grafting typically takes longer to heal than traditional skin grafting because it involves in vitro expansion of the micrografts [9]. Meek skin grafting has been shown to have a higher success rate than traditional skin grafting in burns and chronic wounds [13,14]. Overall, Meek skin grafting may be a better option for patients with larger or more complex wounds, while traditional skin grafting may be sufficient for smaller wounds.

Recently, several studies reported in the literature have claimed that the auxetic skin graft patterns show higher expansion and cover larger burn sites compared to traditional skin grafts [15–17]. Auxetic hierarchical structures, which may induce higher expansion associated with auxetic patterns, might be used for skin graft design [18–21]. Also, for fabricating high-expansion skin grafts auxetic materials can be used, which have shown high expansion and negative Poisson's ratio (NPR). These materials exhibit different properties derived from natural materials. Hierarchical metamaterials also show an NPR with higher strengths. In 2022, Gupta et al. [12] computationally designed different patterns of skin grafts with auxetics and understood the effect of structural changes on expansions. In their study, they observed that auxetic skin graft designs show higher enlargements compared to traditional skin graft-based incisions. In line with this study, several structural and parametric studies were conducted with the alternating slit (AS), rotating triangle (RT), and I-shaped incision patterns with varying variations in slit dimensions, orientations and optimized structural parameters for high expansion. For AS and I-shaped auxetic skin graft patterns, increasing the spacing between adjacent slits decreased the expansion ratios. Increasing the angle for RT-shaped skin graft models decreased the expansion ratio. Several other key findings indicated that mixing auxetic structures or testing grafts with more advanced hierarchical structures may improve the expansions even more.

Hierarchical metamaterial refers to an engineered material with a hierarchical or multi-scale structure, composed of multiple levels of organization or arrangement [22,23]. This term refers to materials that are designed to exhibit distinct and enhanced properties by optimizing the interactions and arrangements of their constituent elements at various length scales. Negative Poisson's ratio materials, in contrast to ordinary materials, exhibit lateral expansion when subjected to stretching. These materials, often referred to as anti-rubber, auxetic, or metamaterials, were initially developed by Rod Lakes [24,25]. The discovery and subsequent study of negative Poisson's ratio foams have opened up new possibilities for the design and application of innovative materials with unique mechanical properties. These materials have garnered significant interest and attention in the scientific community due to their unconventional behavior and potential for various practical applications. Figure 1 shows the tensile and compressive structural behavior of non-auxetic and auxetic structures. [26].

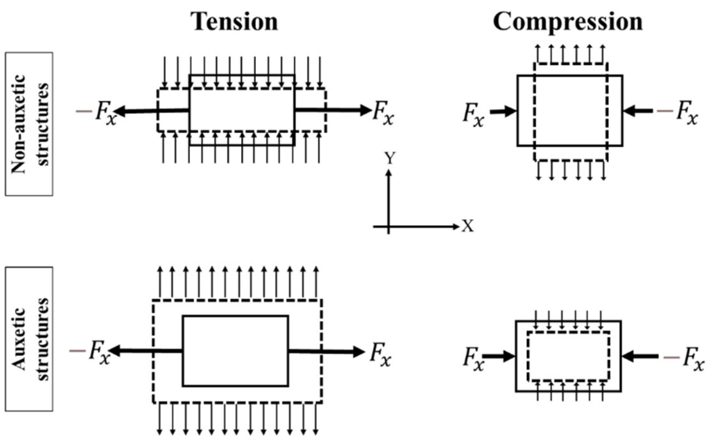

Figure 1. Structural behavior of non-auxetic and auxetic structures under tensile and compressive loadings. Reprinted from [26].

Karathanasopoulos et al. [27] analyzed the mechanical properties of two-dimensional artificial materials under small deformations. They studied different unit cell arrangements and analyzed the differences in their bulk and shear behaviors. Additionally, inner material architecture with varying resistance to pressure and shear loads were calculated. Sorrentino et al. [28] studied bio-inspired rotating squares, rotating squares unit with ligaments, anti-tetrachiral honeycomb and chiral architecture with hollow unit auxetic and analyzed the off-axis mechanical behavior of these mechanical metamaterials. Reis et al. [29] studied the genetic algorithm-based inverse metamaterial design method. In their study, additive manufacturing-based inversely engineered metamaterials were fabricated and tested to experimentally understand the effect of stress distribution. Several computational studies were conducted which analyzed the stress distribution, Poisson's ratio, and deformation [30–34].

Till date, no prior investigations have been conducted, either computationally or experimentally, which shows the realistic loads experienced in a clinical setting (i.e., biaxial testing). This work focuses on the design and computational analysis of complex hierarchical structures of skin grafts up to level 3, incorporating both auxetic and traditional skin graft patterns. The aim is to simulate realistic loads faced in clinical settings, by specifically applying a biaxial loading condition. The computational results were further validated by comparing them with previous experimental findings.

2. Materials and Methods

2.1. Geometrical Modeling

In this work, the computational designs of hierarchical skin graft were examined extensively to cover a large area with the hierarchical skin graft structures. The hierarchical structure shown in Figure 2 is an extension of a 2D unit cell based on previous studies [18]. In the literature, Han et al. [35] developed the unit cell of hierarchical patterns with increasing order of hierarchy with metallic glass and studied their programable stretchability. In another work, Han et al. [12] studied the stretchability using conductor-based silver composite auxetic structures. Several other studies also showed that the hierarchical structures can generate very high expansions [21,22,36–38]. Here, six different skin graft structures were designed on the two-layer skin graft with a length and width of 35 mm. The dimensions of the designs were taken from the literature on hierarchical architectures which shows high expansions [21,22]. The selection of the specific length was based upon the ratios taken from the slit length and slit thickness. From the prior studies [18], the thicknesses of the layers were selected as 0.1 mm (epidermis) and 1.9 mm (dermis). The skin graft models were designed using SolidWorks 2019 (Dassault Systèmes, Vélizy-Villacoublay, France) software and further analyzed using ANSYS Workbench 19 R1 (Ansys, Inc., Canonsburg, PA, USA), as shown in Figure 2. The first, third, and fifth designs were conventional graft structures [39] with a hierarchy of order 1st, 2nd, and 3rd, respectively, as shown in Figure 2a,c,e. The second, fourth, and sixth designed structures were inspired by auxetic skin graft models [34] with a hierarchy of 1st, 2nd, and 3rd order, respectively, as shown in Figure 2b,d,f. The length and gap of all skin graft designs are listed in Table 1. The first design was a traditional skin graft model (Figure 2a) with the same size vertical slits. In the second design (Figure 2b), the slits were oriented perpendicularly to each other with the same gap between the slits. The third and fourth designs were 2nd order hierarchical, traditional, and auxetic skin graft models, respectively (Figure 2c,d). In these designs, the slits were increased with the same area but with different sizes. Similarly, for other designs, the number of slits increased with the same area and hierarchy of order 3, as shown in Figure 2e,f.

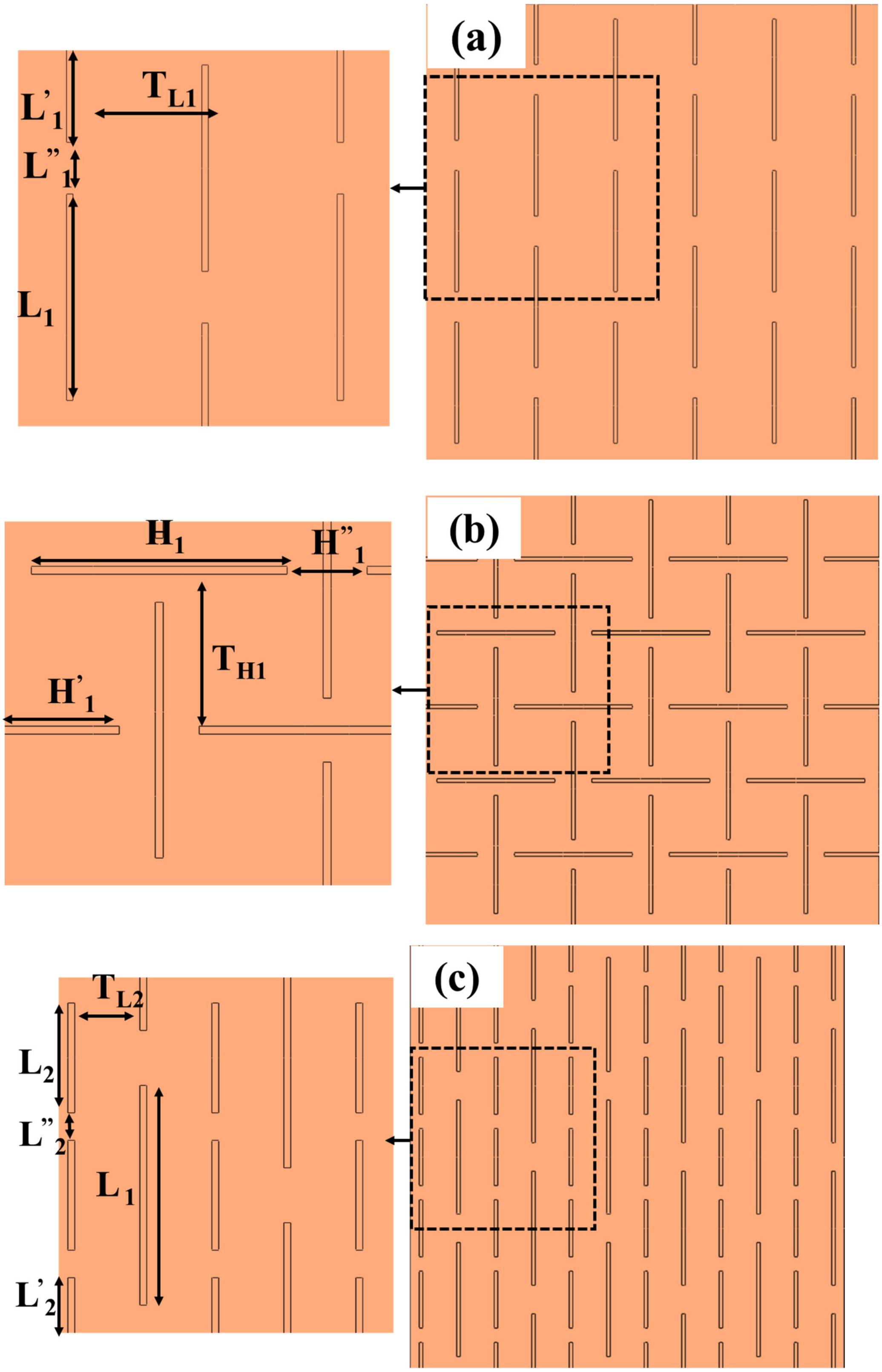

Figure 2. *Cont.*

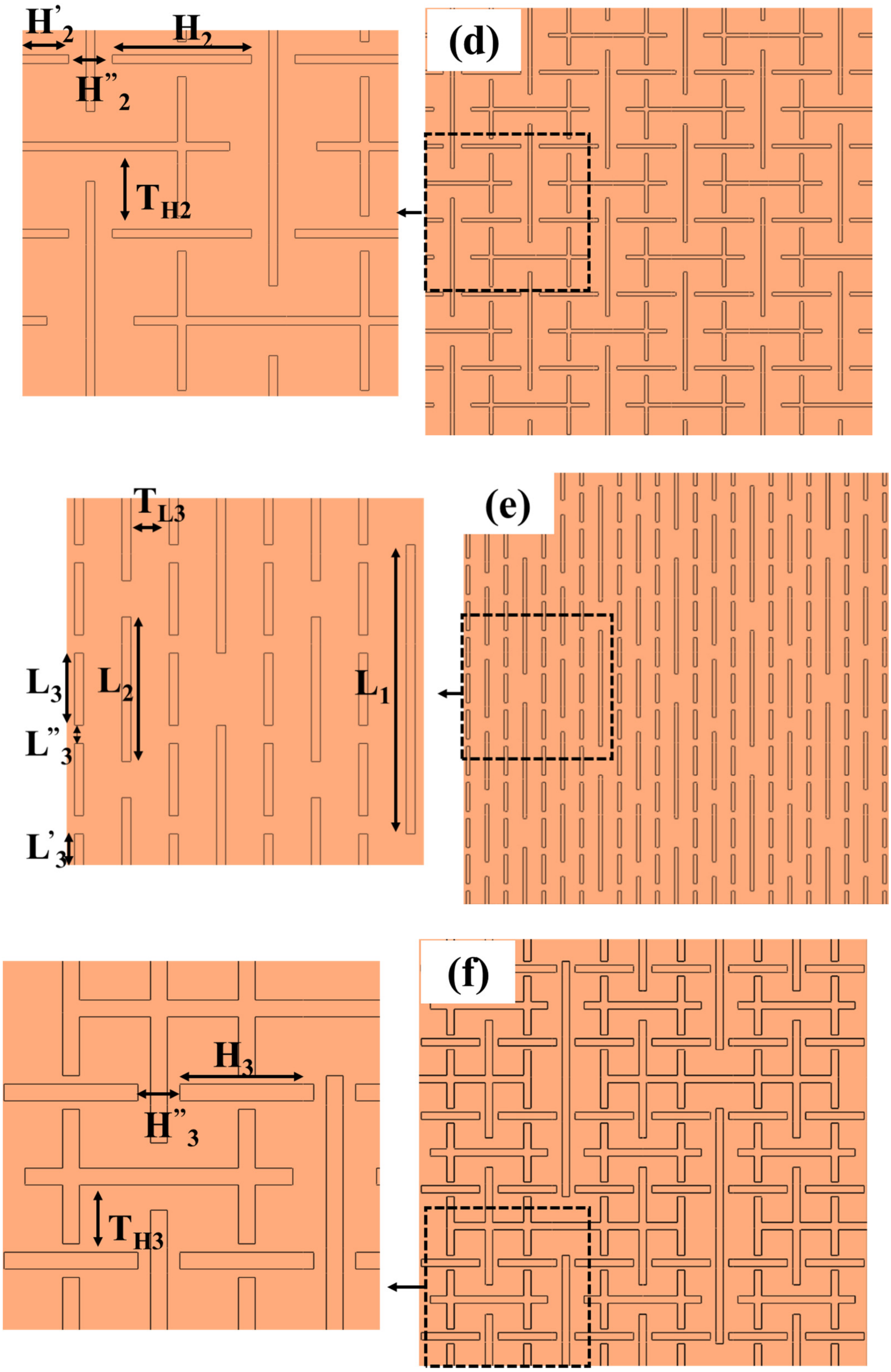

Figure 2. Skin graft models with hierarchical patterns. (**a**) 1st order traditional skin graft, (**b**) 1st order auxetic skin graft, (**c**) 2nd order traditional skin graft, (**d**) 2nd order auxetic skin graft, (**e**) 3rd order traditional skin graft, (**f**) 3rd order auxetic skin graft.

Table 1. Hierarchical skin graft parameters.

Design	Parameters in mm			
1st order traditional grafts	$L_1 = 8.96$	$L'_1 = 4.48$	$L''_1 = 2.24$	$T_{L1} = 5.6$
1st order auxetic grafts	$L_2 = 4.48$	$L'_2 = 2.24$	$L''_2 = 1.12$	$T_{L2} = 2.8$
2nd order traditional grafts	$L_3 = 2.24$	$L'_3 = 1.12$	$L''_3 = 0.56$	$T_{L3} = 1.4$
2nd order auxetic grafts	$H_1 = 8.96$	$H'_1 = 4.48$	$H''_1 = 2.24$	$T_{H1} = 5.6$
3rd order traditional grafts	$H_2 = 4.48$	$H'_2 = 2.24$	$H''_2 = 1.12$	$T_{H2} = 2.8$
3rd order auxetic grafts	$H_3 = 2.24$	$H'_3 = 1.12$	$H''_3 = 0.56$	$T_{H3} = 1.4$

2.2. Material Modeling

In this study, the skin was modeled as an isotropic and elastic material, following the approach employed in previous studies [40]. The aim was to primarily investigate the influence of hierarchy in auxetic and conventional skin graft patterns on a two-layer skin model. However, it is important to acknowledge that real human skin consists of multiple layers, such as fibers, follicles, vessels, and fat, resulting in an anisotropic and non-linear material property. To address this complexity, a recent study by Capek et al. [41] was reviewed which utilized finite element methods (FEMs) to examine the significance of the orientation of Langer's lines. By comparing the deformations in perpendicular and parallel orientations of the graft, small differences were observed in the expansion due to anisotropy. Also, it has been observed in experiments that the stress–strain responses of skin up to 100% stretch can be assumed to be linear, followed by stiffening with further stretching, which has been adopted across many computational studies on skin [42]. Table 2 in this study presents the material properties of the skin layers that were used in the finite element analysis (FEA). The modulus of elasticity, which is a measure of the stiffness of the epidermis and dermis layers, was set at 1 MPa and 4.35 MPa, respectively. In this FEA analysis, the Poisson's ratio was set to 0.46 for the epidermis layer and 0.48 for the dermis layer, which represents the extent of lateral contraction when the material is subjected to axial loading. Also, an upper bound or ultimate tensile strength (UTS) was employed as a threshold, with a value of approximately 27 MPa [34] for assessing skin damage. In the literature, Gupta et al. [41] used the same material properties to understand the effect of length and other dimensional parameters of auxetic and structures. Similarly, Capek et al. [34,40,43] analyzed expansion variations that were assessed by evaluating the displacements in parallel and perpendicular angles of skin graft designs.

Table 2. Material properties of two-layer skin graft models.

Skin Layer	Modulus of Elasticity (MPa)	Poisson's Ratio	Refs.
Epidermis	1	0.46	[34,44]
Dermis	4.35	0.48	[30,45,46]

2.3. Finite Element Modeling

The hierarchical skin graft designs were analyzed computationally using ANSYS software. The material properties of the skin layers, as described in Table 2, were assigned to the skin graft models for stress and deformation analysis. To quantitatively assess the effect of hierarchical designs on Poisson's ratios of the skin graft patterns, uniaxial loading was applied in a controlled manner.

In this work, we have tested the skin grafts under uniaxial and biaxial loading conditions similar to in experiments. For uniaxial loading, one side of the graft was fixed with no deformation in all direction (all degrees of freedom will be zero), and opposite sides of the graft was stretched in the X-direction. This approach enabled a detailed study of the deformation behavior and allowed for the determination of Poisson's ratios for the hierarchical skin graft patterns, providing insights into how the hierarchical designs may influence the material properties and mechanical behavior of the skin grafts. For biaxial loading, the sample was stretched in all directions (+X, −X, +Y, and −Y) and center slit was fixed to perform the FEM analysis. In biaxial stretching, all the edges of the graft were expanded, and the deformation and von-Mises stress were estimated. The UTS value of the skin was compared with the maximum stresses computed iteratively across all models and simulated loads. All the hierarchical patterns were tested uniaxially and biaxially for calculating meshing ratios without reaching the UTS of skin. Figure 3A,B show the boundary conditions of uniaxial and biaxial loading.

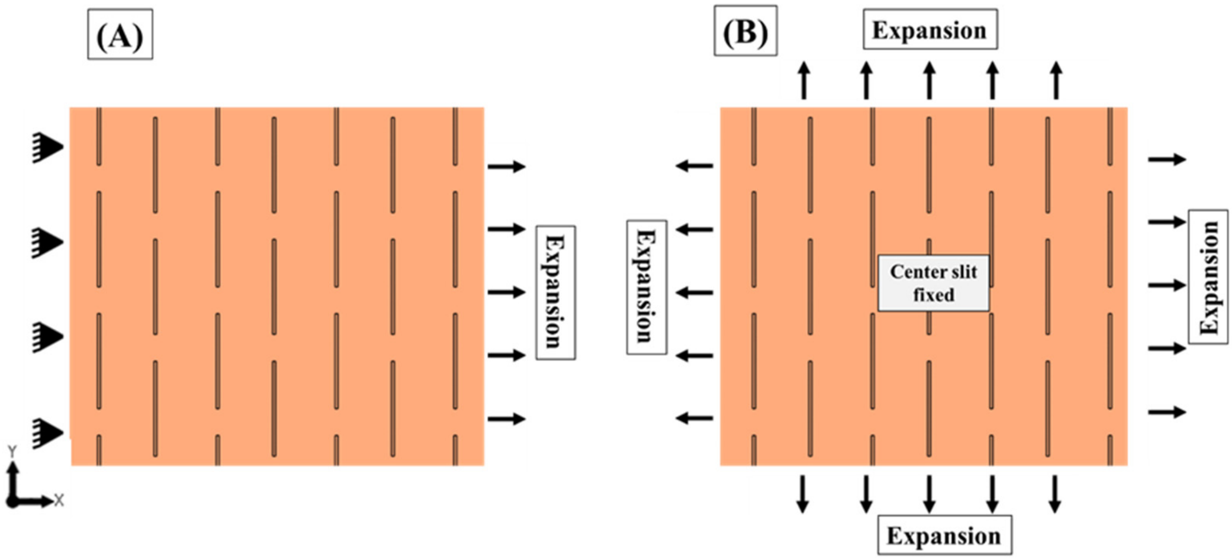

Figure 3. Boundary conditions for (**A**) uniaxial and (**B**) biaxial testing.

2.4. Mesh Convergence Study

In this work, a thorough mesh convergence analysis was conducted to select a mesh size that would generate accurate computational results. To achieve this goal, the percent variation of von-Mises stresses with the change in the number of nodes was quantified, and convergence was considered when the results were within 5% [47,48]. The four meshes with varying levels of fineness, resulting in a total of 57,202, 84,756, 138,180, and 188,475 nodes, respectively, were generated (Figure 4). The results were found to converge by utilizing a mesh size of 0.5 mm, consisting of 138,180 nodes, which was further employed for the computational analysis of the hierarchical skin graft expansion.

To simulate a close fit between the epidermis and dermis layers of skin, we defined a contact pair between the epidermis surface and the dermis surface. The conditions of bonded contact were examined, and the contacts were defined as flexible using the augmented Lagrangian method [49]. A normal penalty stiffness factor of 0.92 and a penetration tolerance factor of 0.08 were utilized. Initial penetration and surface offset were set to null on the contact surface. Additionally, an automatic contact adjustment for gap closure and penetration reduction was implemented in the contact representation. Additionally, to conduct the mesh convergence study, we applied displacements of 35 mm, 70 mm, and 140 mm, and observed the maximum von Mises stress generated in the skin grafts (Figure 5). Based on the results, we selected the optimal mesh (138,180 nodes and 40,784 elements) for subsequent analysis.

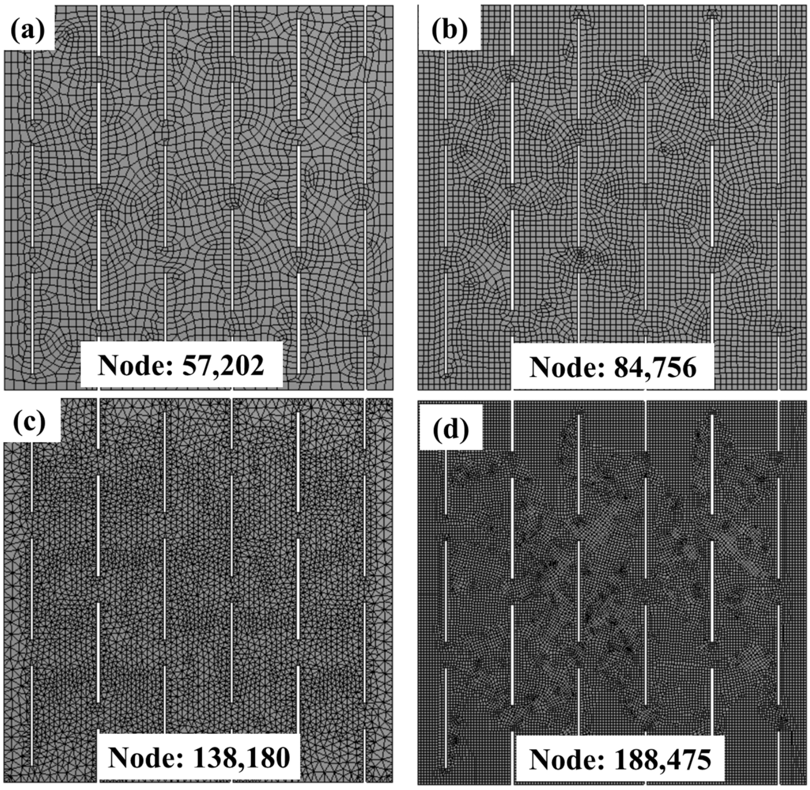

Figure 4. Mesh convergence study with varying lodes. (**a**) very coarse meshing, (**b**) coarse meshing (**c**) fine meshing, (**d**) very fine meshing.

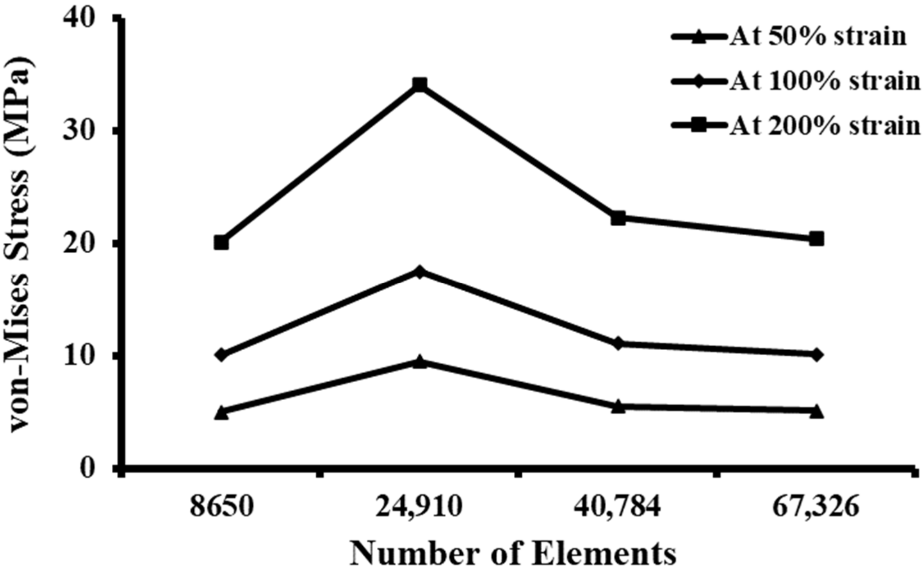

Figure 5. Maximum von-Mises stress versus number of mesh elements for different stains.

2.5. Expansion Estimation

In this study, a comprehensive analysis of the hierarchical conventional and auxetic structure of skin graft designs was attained by determining the meshing ratios and effective Poisson's ratio. The effective Poisson's ratio was estimated through examination of the correlation between longitudinal and lateral strains, which were calculated by comparing changes in length to the initial length. The meshing ratio (MR) was estimated as the ratio of the stretched graft area to the unstretched graft area. MR values were computed for both biaxial and uniaxial constraints, covering the entire range of loading conditions up to the ultimate tensile strength (UTS), as depicted in Figure 6. These quantitative analyses provided valuable insights into the hierarchical behavior of the skin graft designs, elucidating their mechanical characteristics and performance under various loading conditions.

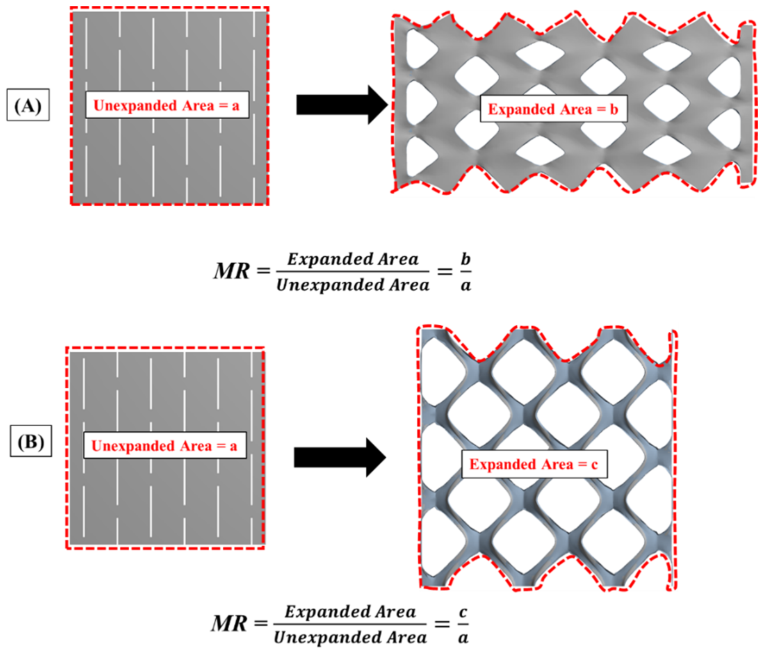

Figure 6. Meshing ratios for (**A**) uniaxial and (**B**) biaxial loading.

3. Results

In this work, six different hierarchical structures, including both conventional and auxetic skin graft designs were modeled with increasing order of hierarchy, and von-Mises stress, Poisson's ratio, and expansion potential were calculated computationally. These two-layer skin graft models were designed using 3D modeling software to analyze their expansion and stress distribution under uniaxial and biaxial loading conditions. The determined expansion of hierarchical structures was bilateral in nature for both uniaxial and biaxial expansion. In clinical settings of skin graft experiments, the meshed skin is similarly stretched up to its maximum limit and stapled in all the sides like in the biaxial tests.

3.1. Uniaxial Expansion

Figure 7 depicts the overall expansion of hierarchical graft patterns for expansion to twice the length in the direction of the X-axis. The X, Y-directional, and total deformation were calculated using ANSYS. The 1st order auxetic skin graft showed maximum deformation (i.e., 41.27 mm) followed by the 3rd order (i.e., 38.39 mm) and 2nd order (i.e., 30.38 mm) auxetic graft patterns in the Y-direction. In conventional skin grafts, 1st, 2nd, and 3rd order showed a reduction of 7.9 mm, 6.28 mm, and 4.84 mm, respectively, in the Y-direction. The total deformation ranged from 35.05 mm to 46.91 mm, depending on the design. For total deformation, conventional skin graft with 2nd order and skin graft with auxetics with 3rd order showed the min. and max. deformation, respectively. In traditional skin grafts, a uniform void area was distributed, and for auxetic skin grafts, a non-uniform void area was distributed, as shown in Figure 7. Auxetic skin grafts with 1st order showed the smallest void area and 3rd order auxetic skin grafts showed the largest void area. It can be concluded that auxetic skin grafts with 1st order may be a suitable configuration over the other models to cover large burn sites during uniaxial stretching.

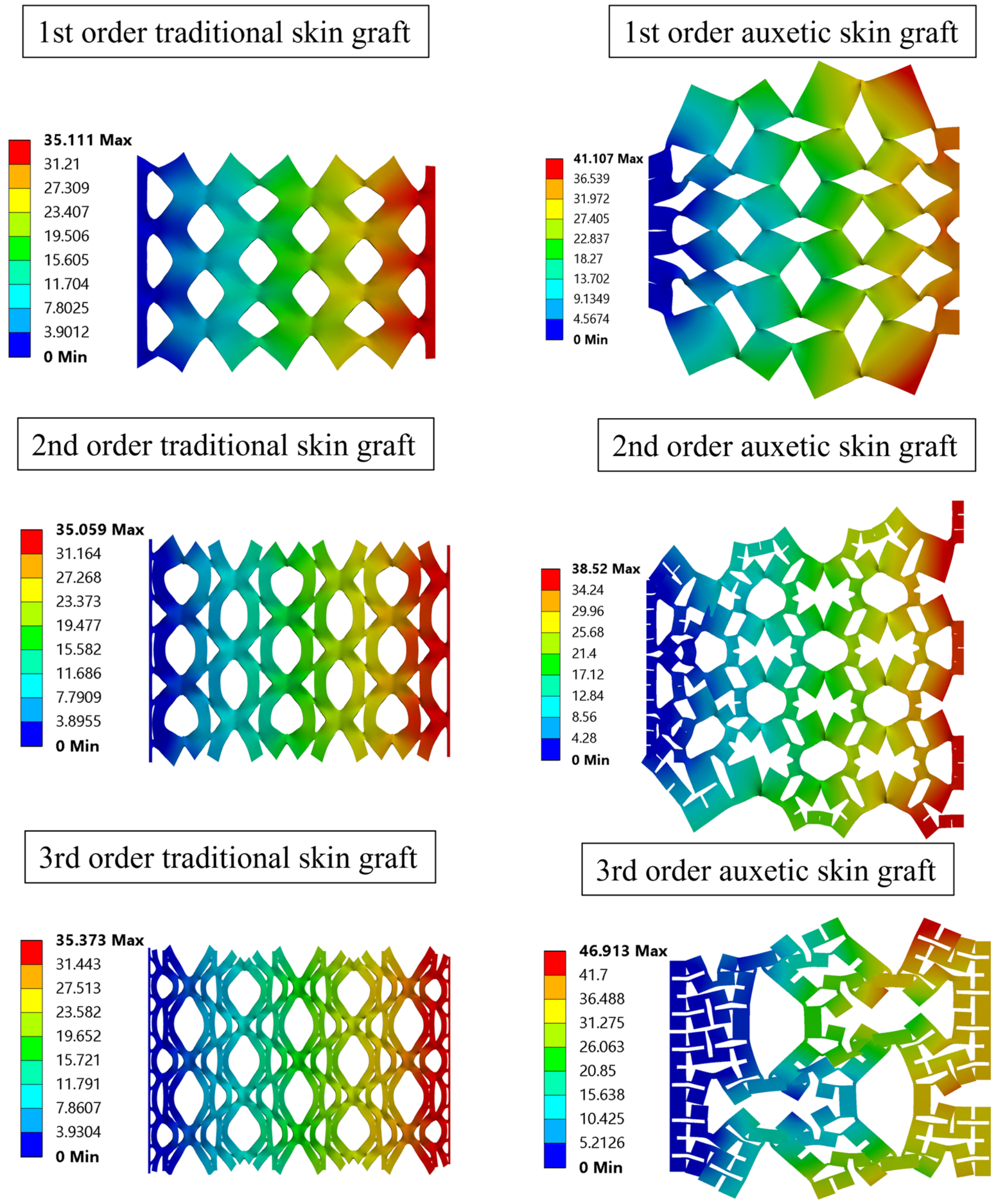

Figure 7. Hierarchy of skin graft models with total deformation (in mm) at 100% expansion.

Table 3 lists the values of the Poisson's ratio (PR) and uniaxial meshing ratio (MR) for the hierarchical skin graft designs at 100% stretching. All the traditional skin grafts showed positive Poisson's ratios of 0.18 ± 0.05 and meshing ratios of 1.77 ± 5%. For the auxetic skin graft models, the value of PR and MR were within the range of −0.86–1.31 and 3.15–4.15, respectively. For all traditional and auxetic skin graft models, with an increase in hierarchy, the Poisson's ratios decreased. In the 1st order, traditional skin grafts showed the minimum meshing ratio, and auxetic skin grafts exhibited the maximum meshing ratio. The 2nd and 3rd order of traditional skin graft models showed increasing meshing ratio with increasing hierarchy. However, in the 2nd and 3rd order skin graft with auxetic models, the ratio of meshing decreased with increasing hierarchy. Graft models with auxetic and first-order properties exhibited the highest values of the ratio.

Table 3. Hierarchical skin graft patterns with average Poisson's and uniaxial meshing ratios.

Skin Graft Model	Avg. Poisson's Ratio	Meshing Ratio (MR) at 100% Strain
1st order traditional grafts	0.22	1.71
1st order auxetic grafts	−1.07	4.15
2nd order traditional grafts	0.18	1.77
2nd order auxetic grafts	−0.76	3.15
3rd order traditional grafts	0.14	1.83
3rd order auxetic grafts	−0.81	3.43

3.2. Biaxial Expansion

The results presented in Figure 8 illustrate the expansion behavior of hierarchical skin graft patterns under biaxial stretching at 100% elongation. The hierarchical designs, including both traditional and auxetic patterns, exhibited significant changes in expansion behavior with increasing hierarchy. Specifically, the 1st and 3rd order hierarchical auxetic skin graft models displayed the min. and max. void areas, respectively. In the hierarchy of designs, the examined gaps were found to be relatively large, which could pose challenges for cell proliferation during wound healing in certain models. The observed expansion patterns may have implications for the effectiveness of these skin graft patterns in promoting wound healing and tissue regeneration. Notably, the 3rd order auxetic skin graft patterns demonstrated the highest expansions under biaxial loadings among all the tested models.

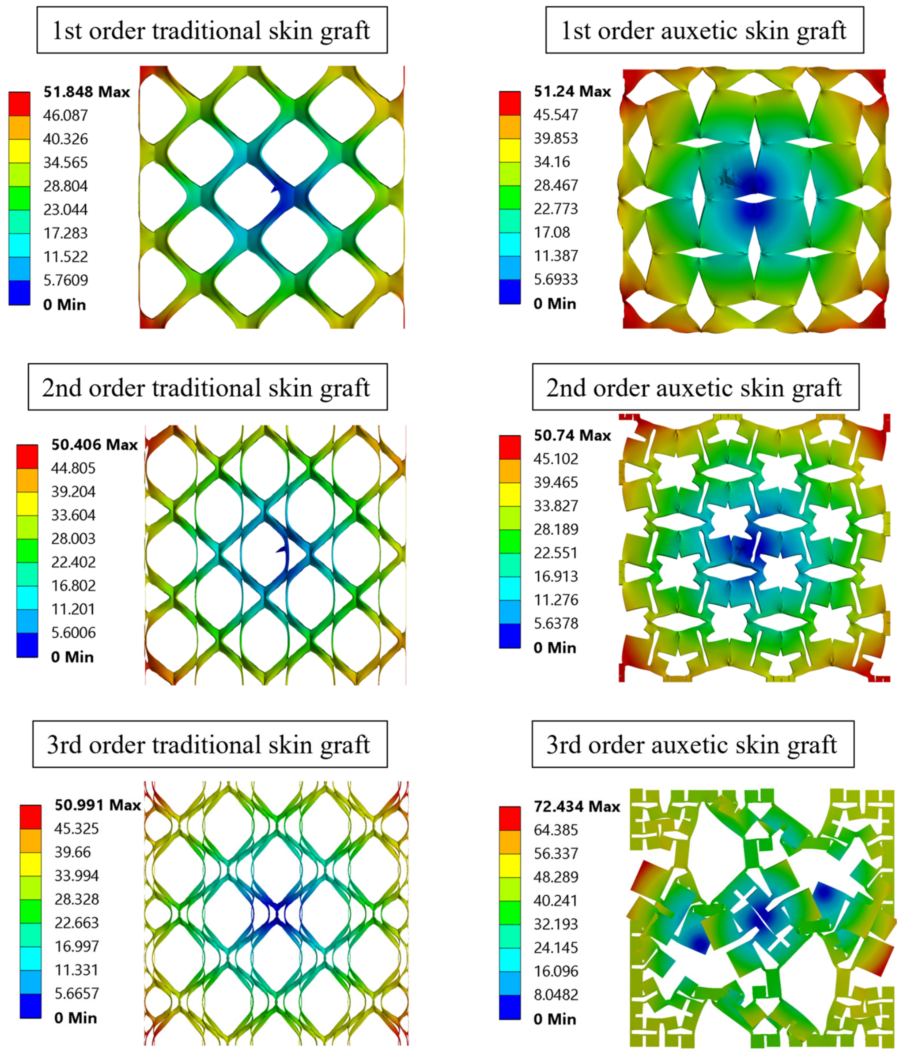

Figure 8. Biaxial expansion (in mm) of hierarchical skin graft patterns at 100% strain.

The max. possible meshing ratio (MR) was calculated for all the hierarchal skin graft models with 1st, 2nd, and 3rd order conventional and auxetic structures by testing uniaxially and biaxially, as shown in Figure 9. The MR values ranged from 1.71 to 4.15 across the graft models while stretching uniaxially. In uniaxial expansion, the highest MR was estimated for the 1st order hierarchy of the auxetic skin graft model. Under biaxial expansion, the MR values ranged from 5.24 to 8.36 across all the models. The maximum MR value was estimated for the hierarchy of 3rd order skin graft models with auxetics. Across all models, the 3rd order skin graft patterns exhibited the maximum MR values for biaxial loadings.

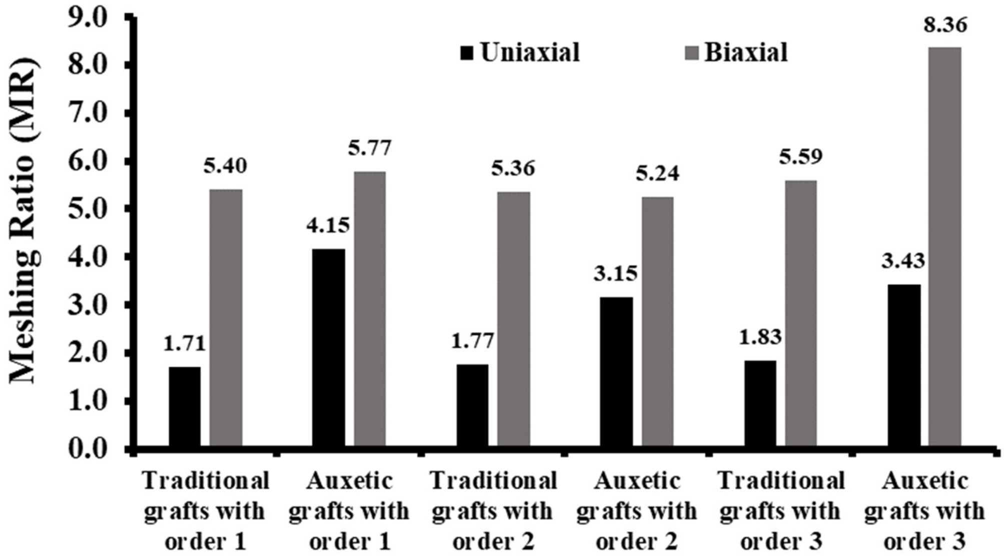

Figure 9. Maximum MR values for hierarchical skin graft patterns at 100% expansion.

3.3. Induced Stresses

The max. von-Mises stresses were calculated for hierarchical skin graft designs under biaxial and uniaxial elongation up to 100%, as shown in Figure 10. In uniaxial expansion, the values of stress were lower compared to biaxial stretching. Among the uniaxial stretching models, the 3rd and 2nd order auxetic skin grafts exhibited the max. and min. stress values, respectively. Similarly, among the biaxial stretching models, the 1st order conventional graft model designs exhibited the highest values of stress, while the 3rd order hierarchical auxetic skin grafts showed the highest stress values. A horizontal strength line in red color at 27 MPa represents the maximum tensile strength of the skin. Skin grafts with stress values below this line are suitable for skin grafting applications, as they are expected to withstand mechanical loads without fracture. However, grafts with stress values above the maximum tensile strength may not be suitable for skin grafting applications, as they may result in skin rupture. Throughout all the tested models, the 2nd order skin graft patterns exhibited the minimum stress values for both uniaxial and biaxial loadings. This indicates that the 2nd order auxetic skin graft pattern may be the most favorable configuration for achieving high expansions without risking skin rupture, making it a potential candidate for skin grafting applications with higher expansion requirements.

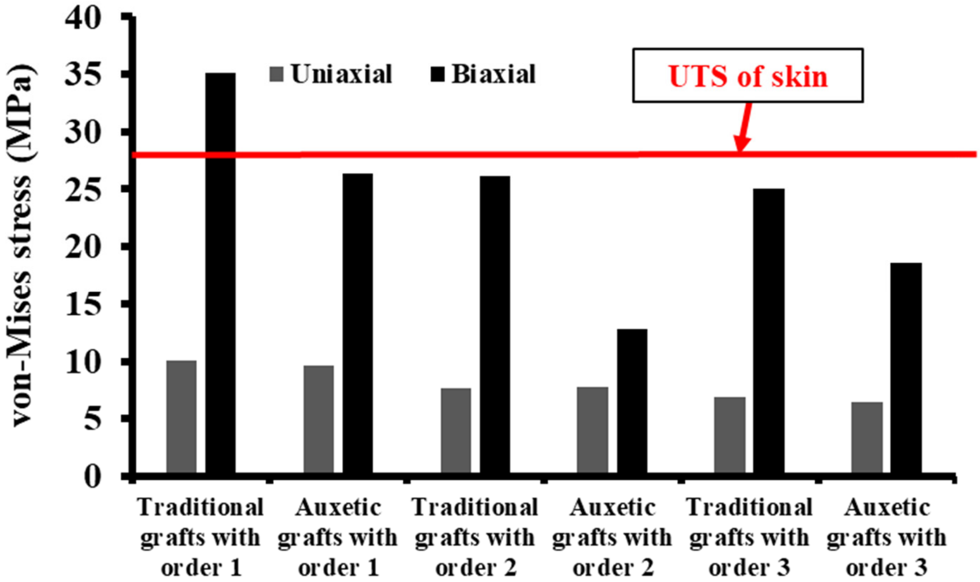

Figure 10. von-Mises stress analysis of hierarchical skin graft models at 100% expansion.

4. Discussions

This work aimed to design hierarchical skin graft patterns and analyze them computationally, which has the potential to revolutionize the field of dermatology. This study presents an innovative technique that utilizes hierarchical auxetic incisions to expand skin grafts, which has shown promising results in increasing the surface area of skin grafts without causing any significant damage to the underlying tissues. A 3D modeling software was used to design these different hierarchical skin graft patterns. A mesh convergence study was performed to generate accurate results. Similar to skin grafting experiments, the same boundary conditions were applied computationally, and the results were analyzed. Structural expansion, meshing, Poisson's ratio, and stress vs. strain responses were calculated under both loading conditions.

In uniaxial stretching, auxetic graft patterns with 1st order showed the lowest void area, and it can be concluded that auxetic skin grafts with 1st order may be a suitable configuration over the other models to cover large burn sites during uniaxial stretching. A similar study was performed by Gupta et al. [41] to understand the expansion of polymer-based hierarchical skin grafts. In their study, hierarchical synthetic skin grafts were developed and tested uniaxially. From the results, they conclude that with increasing level of the hierarchy, the chances of rupture increases. Capek et al. [50] also performed a finite element analysis on traditional skin grafts with varying Langer lines orientation. In their study, they conclude that fiber orientation in the direction of stretching shows relatively higher expansion. Similarly, Gupta et al. [19,36,51] conducted a computational study of traditional skin grafts with modifying slit orientation to understand the biomechanics of skin graft orientation. In their study, 60° slit angle is stated to be the optimum angle for maximum expansion.

In the 3rd order of hierarchy, the auxetics exhibit the maximum porosity, primarily due to a large slit gap. However, in comparison, the 2nd order auxetics did not experience a drastic increase in slit dimensions and gaps. Consequently, the porosity observed in the 2nd order auxetics was comparable to that of traditional grafts. These findings emphasize the significance of considering the hierarchical nature of skin graft designs and their impact on expansion. The results suggest that higher-order auxetic patterns may offer greater expansion potential, but it is crucial to exercise caution when designing hierarchical structures to ensure the presence of adequate optimum voids for effective wound healing. Further studies and optimization of hierarchical skin graft designs may be necessary to enhance their potential for clinical applications.

According to the literature and manufacturers, the max. MR values at 100% uniaxial strain should be 2. As the strain exceeds 100%, the epidermis will expand, and the chance of rupture will increase. At 100% uniaxial strain, the maximum MR value was found to be 4.15 in first-order hierarchical auxetic patterns, with a maximum induced stress of 7.19 MPa, which was much lower than the ultimate tensile strength (UTS) of the skin (i.e., 27 MPa) [52,53].

This study shows the mechanical characteristics of hierarchical auxetic structures, which have the ability to expand in all directions when subjected to external forces [54,55]. The FEA simulations allowed for a better empathetic of the deformation behavior of the expanded hierarchical skin grafts, and this study demonstrated that the hierarchical design of the incisions allows for a controlled expansion of the skin grafts, which can be regulated by adjusting the degree of auxeticity [41,56,57]. The findings of this study have important implications for improving burn surgery outcomes. The current methods used for skin grafting involve the transplantation of a limited amount of skin, which often results in insufficient coverage of the affected area [41,56,57]. The hierarchical auxetic incisions technique, on the other hand, allows for the expansion of the skin grafts without compromising their integrity, thus providing a larger surface area for skin coverage.

A few limitations of this study need to be acknowledged. In this work, the FEA simulations were based on certain assumptions and simplifications and may not fully capture the complexity of the mechanical characteristics of skin grafts in vivo conditions (e.g., a square shape sample with constant thickness was used in this study). Also, biological and chemical factors like blood clotting, wound bed preparation, cell growth were difficult to simulate in the computational study. Additionally, linear and isotropic mechanical properties were adopted for the skin in the applied stretch range, in line with observations in the previous literature. In the future, incorporating the anisotropic effects using nonlinear hyperplastic models may improve the accuracy of the results. Also, skin with varying thicknesses and shapes, and from different body locations must be investigated with the skin graft patterns to study their roles in graft expansion.

5. Conclusions

In conclusion, this study investigated the hierarchical configuration of auxetic and traditional skin graft models to compare their expansion potentials. Uniaxial and biaxial loading tests were performed for analyzing the maximum stretching limit of skin to estimate enlargement potentials and stress values of the skin graft patterns. In uniaxial loading, non-positive Poisson's ratio (NPR) values were quantified for graft models with hierarchical auxetic patterns, while positive values were estimated for traditional graft models with hierarchical patterns. Graft models with auxetics and single hierarchical order demonstrated the highest NPR of -1.07 and the meshing ratio of 4.15 at 100% longitudinal strain. Biaxially, hierarchical traditional skin graft models produced large void areas, significantly higher than that in the hierarchical graft models with auxetics. Graft models with auxetics and single hierarchical order showed the least amount of voids, which is expected to promote the healing of wounds. Moreover, when the designs were stretched till the maximum stretch limit of skin, the expansions with a meshing ratio significantly larger compared to the conventional graft patterns (i.e., >3) were generated.

Across all the skin graft models, the 1st order hierarchical auxetic model demonstrated the highest meshing ratio under uniaxial loading and the highest meshing ratio without voids under biaxial loading. These findings suggest that the 1st order auxetic skin graft pattern has the potential to obtain a substantial area of skin grafting using limited amounts of healthy skin, which could be invaluable for improving burn surgery outcomes. A further experimental investigation is warranted to validate these results and explore the feasibility of utilizing hierarchical skin graft patterns for clinical applications. The fabrication of skin graft designs with higher expansion potentials and minimal void areas could potentially revolutionize burn surgery techniques and contribute to improved patient outcomes.

Author Contributions: V.G.: literature; conceptualization; design; analysis; original draft writing. A.C.: supervision; conceptualization; editing; draft editing and reviewing. All authors have read and agreed to the published version of the manuscript.

Funding: This research received no external funding.

Institutional Review Board Statement: Not applicable.

Informed Consent Statement: Not applicable.

Data Availability Statement: Not applicable.

Acknowledgments: This paper and the research would not have been possible without the exceptional support of my supervisor (A.C.) and facilities provided by the Indian Institute of Technology Delhi (IIT-D), India.

Conflicts of Interest: The authors declare no conflict of interest.

References

1. Singh, G.; Chanda, A. Mechanical properties of whole-body soft human tissues: A review. *Biomed. Mater.* **2021**, *16*, 062004. [CrossRef] [PubMed]
2. Snyder, D.E.; Sapper, E.D.; Tornabene, F.; Snyder, D.E.; Sapper, E.D. See Me, Feel Me, Touch Me, Heal Me: A Contextual Overview of Conductive Polymer Composites as Synthetic Human Skin. *J. Compos. Sci.* **2022**, *6*, 141. [CrossRef]
3. Sakamoto, M.; Morimoto, N.; Inoie, M.; Takahagi, M.; Ogino, S.; Jinno, C.; Suzuki, S. Cultured Human Epidermis Combined with Meshed Skin Autografts Accelerates Epithelialization and Granulation Tissue Formation in a Rat Model. *Ann. Plast. Surg.* **2017**, *78*, 651. [CrossRef]
4. Chen, A.I.; Balter, M.L.; Chen, M.I.; Gross, D.; Alam, S.K.; Maguire, T.J.; Yarmush, M.L. Multilayered tissue mimicking skin and vessel phantoms with tunable mechanical, optical, and acoustic properties. *Med. Phys.* **2016**, *43*, 3117–3131. [CrossRef] [PubMed]
5. Holmdahl, V.; Backman, O.; Gunnarsson, U.; Strigård, K. The Tensile Strength of Full-Thickness Skin: A Laboratory Study Prior to Its Use as Reinforcement in Parastomal Hernia Repair. *Front. Surg.* **2019**, *6*, 69. [CrossRef]
6. WHO—World Health Organization. Burns. Available online: https://www.who.int/ (accessed on 1 July 2022).
7. Noor, A.; Afzal, A.; Masood, R.; Khaliq, Z.; Ahmad, S.; Ahmad, F.; Qadir, M.B.; Irfan, M. Dressings for burn wound: A review. *J. Mater. Sci.* **2022**, *57*, 6536–6572. [CrossRef]
8. Jeschke, M.G.; van Baar, M.E.; Choudhry, M.A.; Chung, K.K.; Gibran, N.S.; Logsetty, S. Burn injury. *Nat. Rev. Dis. Prim.* **2020**, *6*, 11. [CrossRef]
9. Noureldin, M.A.; Said, T.A.; Makeen, K.; Kadry, H.M. Comparative study between skin micrografting (Meek technique) and meshed skin grafts in paediatric burns. *Burns* **2022**, *48*, 1632–1644. [CrossRef]
10. Rijpma, D.; Claes, K.; Hoeksema, H.; de Decker, I.; Verbelen, J.; Monstrey, S.; Pijpe, A.; van Zuijlen, P.; Meij-de Vries, A. The Meek micrograft technique for burns; review on its outcomes: Searching for the superior skin grafting technique. *Burns* **2022**, *48*, 1287–1300. [CrossRef]
11. Lari, A.R.; Gang, R.K. Expansion technique for skin grafts (Meek technique) in the treatment of severely burned patients. *Burns* **2001**, *27*, 61–66. [CrossRef]
12. Gupta, S.; Gupta, V.; Chanda, A. Biomechanical modeling of novel high expansion auxetic skin grafts. *Int. J. Numer. Methods Biomed. Eng.* **2022**, *38*, e3586. [CrossRef] [PubMed]
13. Mishra, A.; Rabiee, S.; Opel, S.; Jones, I. Applying the modified Meek technique to heal smaller burns: A retrospective review. *Burn. Open* **2022**, *6*, 120–124. [CrossRef]
14. Koetsier, K.S.; Wong, J.N.; Muffley, L.A.; Carrougher, G.J.; Pham, T.N.; Gibran, N.S. Prospective observational study comparing burn surgeons' estimations of wound healing after skin grafting to photo-assisted methods. *Burns* **2019**, *45*, 1562–1570. [CrossRef]
15. Miranda, A. Auxetic Expansion of the Tunica Albuginea for Penile Length and Girth Restoration without a Graft: A Translational Study. *Sex. Med.* **2021**, *9*, 100456. [CrossRef] [PubMed]
16. Grima, J.N.; Mizzi, L.; Azzopardi, K.M.; Gatt, R. Auxetic Perforated Mechanical Metamaterials with Randomly Oriented Cuts. *Adv. Mater.* **2016**, *28*, 385–389. [CrossRef] [PubMed]
17. Veerabagu, U.; Palza, H.; Quero, F. Review: Auxetic Polymer-Based Mechanical Metamaterials for Biomedical Applications. *ACS Biomater. Sci. Eng.* **2022**, *8*, 2798–2824. [CrossRef]
18. Han, D.X.; Chen, S.H.; Zhao, L.; Tong, X.; Chan, K.C. Architected hierarchical kirigami metallic glass with programmable stretchability. *AIP Adv.* **2022**, *12*, 8–13. [CrossRef]
19. Mazur, E.; Shishkovsky, I. Additively Manufactured Hierarchical Auxetic Mechanical Metamaterials. *Materials* **2022**, *15*, 5600. [CrossRef]
20. Mousanezhad, D.; Babaee, S.; Ebrahimi, H.; Ghosh, R.; Hamouda, A.S.; Bertoldi, K.; Vaziri, A. Hierarchical honeycomb auxetic metamaterials. *Sci. Rep.* **2015**, *5*, 18306. [CrossRef]
21. Tang, Y.; Yin, J. Design of cut unit geometry in hierarchical kirigami-based auxetic metamaterials for high stretchability and compressibility. *Extrem. Mech. Lett.* **2017**, *12*, 77–85. [CrossRef]

22. Gupta, V.; Singh, G.; Chanda, A. Development of novel hierarchical designs for skin graft simulants with high expansion potential. *Biomed. Phys. Eng. Express* **2023**, *9*, 035024. [CrossRef] [PubMed]
23. Dudek, K.K.; Gatt, R.; Mizzi, L.; Dudek, M.R.; Attard, D.; Evans, K.E.; Grima, J.N. On the dynamics and control of mechanical properties of hierarchical rotating rigid unit auxetics. *Sci. Rep.* **2017**, *7*, 46529. [CrossRef]
24. Mizzi, L.; Attard, D.; Evans, K.E.; Gatt, R.; Grima, J.N. Auxetic mechanical metamaterials with diamond and elliptically shaped perforations. *Acta Mech.* **2021**, *232*, 779–791. [CrossRef]
25. Lakes, R.S. Negative-Poisson's-Ratio Materials: Auxetic Solids. *Annu. Rev. Mater. Res.* **2017**, *47*, 63–81. [CrossRef]
26. Gupta, V.; Singh, G.; Gupta, S.; Chanda, A. Expansion potential of auxetic prosthetic skin grafts: A review. *Eng. Res. Express* **2023**, *5*, 022003. [CrossRef]
27. Karathanasopoulos, N.; Dos Reis, F.; Reda, H.; Ganghoffer, J.F. Computing the effective bulk and normal to shear properties of common two-dimensional architectured materials. *Comput. Mater. Sci.* **2018**, *154*, 284–294. [CrossRef]
28. Sorrentino, A.; Castagnetti, D.; Mizzi, L.; Spaggiari, A. Bio-inspired auxetic mechanical metamaterials evolved from rotating squares unit. *Mech. Mater.* **2022**, *173*, 104421. [CrossRef]
29. Dos Reis, F.; Karathanasopoulos, N. Inverse metamaterial design combining genetic algorithms with asymptotic homogenization schemes. *Int. J. Solids Struct.* **2022**, *250*, 111702. [CrossRef]
30. Gupta, V.; Gupta, S.; Chanda, A. Expansion potential of skin grafts with novel rotating triangle shaped auxetic incisions. *Emerg. Mater. Res.* **2022**, *11*, 406–414. [CrossRef]
31. Skatulla, S.; Stark, S. Numerical Aspects of a Continuum Sintering Model Formulated in the Standard Dissipative Framework. *Math. Comput. Appl.* **2023**, *28*, 69. [CrossRef]
32. Ren, X.; Das, R.; Tran, P.; Ngo, T.D.; Xie, Y.M. Auxetic metamaterials and structures: A review. *Smart Mater. Struct.* **2018**, *27*, 023001. [CrossRef]
33. Naik, S.; Dandagwhal, R.D.; Wani, C.N.; Giri, S.K. A review on various aspects of auxetic materials. *AIP Conf. Proc.* **2019**, *2105*, 020004. [CrossRef]
34. Gupta, V.; Chanda, A. Expansion potential of skin grafts with alternating slit based auxetic incisions. *Forces Mech.* **2022**, *7*, 100092. [CrossRef]
35. Han, S.; Jung, S.; Jeong, S.; Choi, J.; Choi, Y.; Lee, S.Y. High-performance, biaxially stretchable conductor based on Ag composites and hierarchical auxetic structure. *J. Mater. Chem. C* **2020**, *8*, 1556–1561. [CrossRef]
36. Gatt, R.; Mizzi, L.; Azzopardi, J.I.; Azzopardi, K.M.; Attard, D.; Casha, A.; Briffa, J.; Grima, J.N. Hierarchical Auxetic Mechanical Metamaterials. *Sci. Rep.* **2015**, *5*, 8395. [CrossRef]
37. Dudek, K.K.; Martínez, J.A.I.; Ulliac, G.; Kadic, M. Micro-Scale Auxetic Hierarchical Mechanical Metamaterials for Shape Morphing. *Adv. Mater.* **2022**, *34*, 2110115. [CrossRef]
38. Gupta, V.; Singh, G.; Chanda, A. Development of hierarchical auxetic skin graft simulants with high expansion potential. *Biomed. Eng. Adv.* **2023**, *5*, 100087. [CrossRef]
39. Luo, C.; Han, C.Z.; Zhang, X.Y.; Zhang, X.G.; Ren, X.; Xie, Y.M. Design, manufacturing and applications of auxetic tubular structures: A review. *Thin-Walled Struct.* **2021**, *163*, 107682. [CrossRef]
40. Gallagher, A.J.; Ní Anniadh, A.; Bruyere, K.; Otténio, M.; Xie, H.; Gilchrist, M.D. Dynamic tensile properties of human skin. In Proceedings of the 2012 IRCOBI Conference Proceedings—International Research Council on the Biomechanics of Injury, Dublin, Ireland, 12–14 September 2012; pp. 494–502.
41. Chanda, A.; Ruchti, T.; Unnikrishnan, V. Computational modeling of wound suture: A review. *IEEE Rev. Biomed. Eng.* **2018**, *11*, 165–176. [CrossRef]
42. Capek, L.; Flynn, C.; Molitor, M.; Chong, S.; Henys, P. Graft orientation influences meshing ratio. *Burns* **2018**, *44*, 1439–1445. [CrossRef]
43. Geerligs, M.; van Breemen, L.; Peters, G.; Ackermans, P.; Baaijens, F.; Oomens, C. In vitro indentation to determine the mechanical properties of epidermis. *J. Biomech.* **2011**, *44*, 1176–1181. [CrossRef]
44. Chanda, A.; Graeter, R.; Unnikrishnan, V. Effect of blasts on subject-specific computational models of skin and bone sections at various locations on the human body. *AIMS Mater. Sci.* **2015**, *2*, 425–447. [CrossRef]
45. Plewa, J.; Płońska, M.; Lis, P. Investigation of Modified Auxetic Structures from Rigid Rotating Squares. *Materials* **2022**, *15*, 2848. [CrossRef]
46. Novak, N.; Vesenjak, M.; Ren, Z. Computational Simulation and Optimization of Functionally Graded Auxetic Structures Made From Inverted Tetrapods. *Phys. Status Solidi Basic Res.* **2017**, *254*, 1600753. [CrossRef]
47. Chethan, K.N.; Ogulcan, G.; Zuber, M.; Shenoy, S. Wear estimation of trapezoidal and circular shaped hip implants along with varying taper trunnion radiuses using finite element method. *Comput. Methods Programs Biomed.* **2020**, *196*, 105597. [CrossRef]
48. Singh, G.; Gupta, V.; Chanda, A. Mechanical Characterization of Rotating Triangle Shaped Auxetic Skin Graft Simulants. *Facta Univ. Ser. Mech. Eng.* **2022**, 1–16.
49. Gupta, V.; Singh, G.; Chanda, A. Finite element analysis of a hybrid corrugated hip implant for stability and loading during gait phases. *Biomed. Phys. Eng.* **2022**, *8*, 035028. [CrossRef] [PubMed]
50. Gupta, V.; Singh, G.; Chanda, A. Development and testing of skin grafts models with varying slit orientations. *Mater. Today Proc.* **2022**, *62*, 3462–3467. [CrossRef]

51. Shen, L.; Wang, X.; Li, Z.; Wei, K.; Wang, Z. Elastic properties of an additive manufactured three-dimensional vertex-based hierarchical re-entrant structure. *Mater. Des.* **2022**, *216*, 110527. [CrossRef]
52. Gupta, V.; Chanda, A. Expansion potential of novel skin grafts simulants with I-shaped auxetic incisions. *Biomed. Eng. Adv.* **2023**, *5*, 100071. [CrossRef]
53. Sheikh, A.A.; Sheikh, S.R.; Admane, S.S. Development and Characterization of Novel. *Asian J. Pharm.* **2017**, *2017*, 616–624. [CrossRef]
54. Abou Neel, E.A.; Bozec, L.; Knowles, J.C.; Syed, O.; Mudera, V.; Day, R.; Hyun, J.K. Collagen—Emerging collagen based therapies hit the patient. *Adv. Drug Deliv. Rev.* **2013**, *65*, 429–456. [CrossRef]
55. Makvandi, P.; Maleki, A.; Shabani, M.; Hutton, A.R.J.; Kirkby, M.; Jamaledin, R.; Fang, T.; He, J.; Lee, J.; Mazzolai, B.; et al. Bioinspired microneedle patches: Biomimetic designs, fabrication, and biomedical applications. *Matter* **2022**, *5*, 390–429. [CrossRef]
56. Henderson, J.; Arya, R.; Gillespie, P. Skin graft meshing, over-meshing and cross-meshing. *Int. J. Surg.* **2012**, *10*, 547–550. [CrossRef]
57. Bogdanov, S.B.; Gilevich, I.V.; Melkonyan, K.I.; Sotnichenko, A.S.; Alekseenko, S.N.; Porhanov, V.A. Total full-thickness skin grafting for treating patients with extensive facial burn injury: A 10-year experience. *Burns* **2021**, *47*, 1389–1398. [CrossRef]